AN EXTENSION OF AN ALGORITHM FOR PLANAR FOUR-BAR PATH GENERATION WITH OPTIMIZATION

Yahia M. Al-Smadi[a], Kevin Russell[b], Wen-Tzong Lee[c], Raj S. Sodhi[d]
[a] *AECOM Special Structures Group, New York, NY 10005, U.S.A*
E-mail: yahia.al-smadi@aecom.com
[b] *Armaments Engineering and Technology Center, US Army Research, Development and Engineering Center, Picatinny, NJ 07806, U.S.A*
[c] *Department of Computer Science and Applications, Leader University, Tainan 70970, Taiwan*
[d] *Department of Mechanical Engineering, New Jersey Institute of Technology, Newark, NJ07102, U.S.A*

Received January 2009, Accepted August 2009
No. 09-CSME-03, E.I.C. Accession 3089

ABSTRACT

This work is an extension of the authors' published work on a planar four-bar motion generation search algorithm with Grashof, transmission angle and linkage perimeter conditions [1]. This latest work considers planar four-bar path generation with a coupler point load, crank static torque, crank transverse deflection and follower buckling in a modified search algorithm. As demonstrated in the example, a conventional methodology used in kinematic path generation has been expanded to consider static loading, elastic deflection and buckling in path generation. These factors must be considered in mechanical design, but are not the focus in traditional kinematic synthesis.

L'EXTENSION D'UN ALGORITHME DE GÉNÉRATION DE TRAJECTOIRE OPTIMISÉ POUR UN QUADRILATÈRE ARTICULÉ PLANAIRE

RÉSUMÉ

L'article est une suite du travail déjà publié sur un algorithme de recherche pour la génération de trajectoire pour un quadrilatère articulé planaire, basé sur la loi Grashof, l'angle de transmission et les conditions de périmètre des liaisons [1]. Ce travail se penche sur la génération de trajectoire avec le chargement d'un point sur la liaison coupleur, la couple statique de manivelle, la déflection transversale de manivelle et le flambage de la liaison suiveur avec un algorithme de recherche modifié. Une méthodologie conventionnelle de génération cinématique de trajectoire, tel que démontré par un exemple, a été améliorée en considérant le chargement statique, la déflection élastique et le flambage. Ces facteurs doivent être considérés dans la conception mécanique, mais ils ne sont pas le point central dans la synthèse cinématique traditionnelle.

1. INTRODUCTION

1.1. Published Works in Synthesis for Rigid-Body Guidance

The synthesis of planar four-bar mechanisms for rigid-body guidance is a well-established field. Recent contributions include the work of Martin et al. [1]. These authors presented a search and selection algorithm to down-select planar four-bar path generators with respect to Grashof conditions, transmission angle conditions and mechanism perimeter conditions. Yao and Angeles [2] applied the contour method in the approximate synthesis of planar linkages for rigid-body guidance. By deriving a set of two bivariate polynomial equations and plotting these equations, the real solution to the optimizations (corresponding to the intersections of the contour plots) is determined. Hong and Erdman [3] presented a method that is applicable for the synthesis of adjustable four-bar planar and spherical mechanisms. Their work shows that nonadjustable mechanism solutions are special cases of adjustable mechanism solutions. Zhou and Cheung [4] introduced an optimal synthesis method for adjustable four-bar motion generators. A modified genetic algorithm is used to seek the global optimal solution of an equation set that includes constraints for fixed pivot positions, no branch defect, crank existence and link length ratios. Al-Widyan et al. [5] considered the robust synthesis of planar four-bar linkages for motion generation. Danieli et al. [6] applied Burmester theory in the design of planar four-bar motion generators to reproduce tibia-femur relative motion. Goehler et al. [7] applied parameterized T_1 motion theory to the synthesis of planar four-bar motion generators. This T_1 motion theory is general and not limited to the second order parameterization that is associated with prior development of T_1 motion theory. Caracciolo and Trevisani [8] considered rigid-body motion control of flexible four-bar linkages. In their work, a discrete finite element model of the four-bar mechanism accounts for geometric and inertial nonlinearities. Zhixing et al. [9] presented a guidance-line rotation method for rigid-body guidance for the synthesis of planar four-bar mechanisms. The method effectively solves the rigid-body guidance synthesis problem for crank–rocker mechanisms, double-rocker mechanisms and double-crank mechanisms for four rigid-body positions and beyond. Lin and Modler [10] presented a method to avoid branch defects, order defects and ensure link rotatability in three-point path generation. The method considers (but is not limited to) planar four-bar mechanisms.

Although planar motion and path generation are well-established fields, the concept of including static structural conditions in rigid-body guidance is not nearly as established. With the exception of Huang and Roth [11] whose work includes analytical motion generation models for planar four-bar mechanisms with a prescribed coupler load, most other works that investigate the structural behavior of a classical planar four-bar mechanism under load do not consider the structural behavior in the context of motion or path generation. The works of Dado [12], Venanzi et al. [13], Sönmez [14], Plaut et al. [15] and Siriam and Mruthyunjaya [16] do consider flexible links and/or buckling in mechanism design, but they consider the design of compliant mechanisms as opposed to classical planar four-bar mechanisms.

1.2. Scope of Work

A coupler load can have a negative effect in path generation since any resulting link deflections can compromise the accuracy of the precision points achieved by the mechanism. This work presents a nonlinear optimization problem and improved search algorithm to

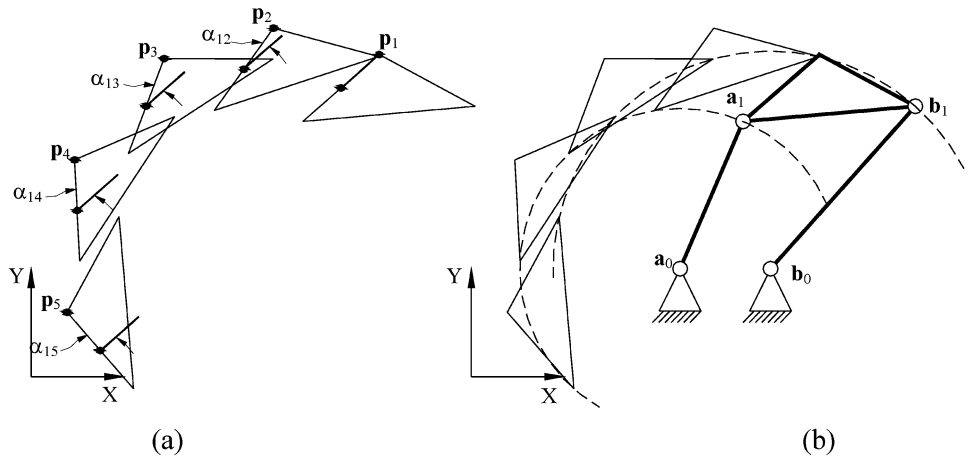

Fig. 1. (a) Prescribed coupler parameters and (b) calculated planar four-bar mechanism.

synthesize planar four-bar path generators with constraints for static loading and link elasticity. The specific constraints included consider static torque of the crank, transverse deflection of the crank and buckling of the follower.

2. PLANAR FOUR-BAR PATH GENERATION

The objective in planar four-bar path generation is to calculate the mechanism dimensions required to achieve or approximate a set of prescribed coupler path points. Figure 1a includes five prescribed coupler path points defined by the x and y-coordinates of the coupler point variable $\mathbf{p}$ and the coupler displacement angle variable α_{1i}. Figure 1b includes the mechanism fixed pivot variables $\mathbf{a}_0$ and $\mathbf{b}_0$ and moving pivot variables $\mathbf{a}_1$ and $\mathbf{b}_1$. The X and Y-coordinates of the fixed and moving pivot variables are the mechanism dimensions to be calculated in path generation.

The planar four-bar path generation model presented by Suh and Radcliffe [17] is expressed as

$$([\mathbf{D}_{1i}]\mathbf{a}_1-\mathbf{a}_0)^T([\mathbf{D}_{1i}]\mathbf{a}_1-\mathbf{a}_0)-(\mathbf{a}_1-\mathbf{a}_0)^T(\mathbf{a}_1-\mathbf{a}_0)=0 \tag{1}$$

$$([\mathbf{D}_{1i}]\mathbf{b}_1-\mathbf{b}_0)^T([\mathbf{D}_{1i}]\mathbf{b}_1-\mathbf{b}_0)-(\mathbf{b}_1-\mathbf{b}_0)^T(\mathbf{b}_1-\mathbf{b}_0)=0 \tag{2}$$

where

$$[\mathbf{D}_{1i}]=\begin{bmatrix}\cos\alpha_{1i} & -\sin\alpha_{1i} & p_{ix}-p_{1x}\cos\alpha_{1i}+p_{1y}\sin\alpha_{1i}\\ \sin\alpha_{1i} & \cos\alpha_{1i} & p_{iy}-p_{1x}\sin\alpha_{1i}-p_{1y}\cos\alpha_{1i}\\ 0 & 0 & 1\end{bmatrix}.\ (i=2,\,3,\,4,\,5) \tag{3}$$

Equation (1) and (2) ensure the constant lengths of the crank and follower links. Equation (3) is a planar coupler displacement matrix. In Equation (3) variables $\mathbf{p}_1$ and $\mathbf{p}_i$ denote a coupler path point in the starting and displaced locations respectively and variable α_{1i} denotes the coupler angular displacement from orientation 1 to orientation i. Because coupler point accuracy is the

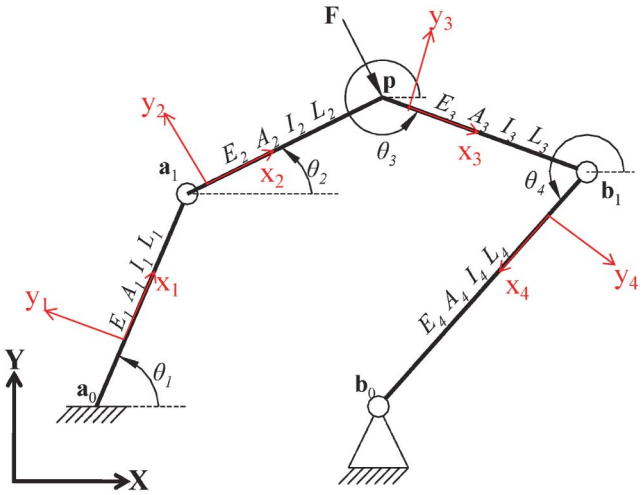

Fig. 2. Statically-loaded planar four-bar mechanism.

focus in path generation, the accuracy of the orientation angles approximated by the synthesized mechanism is not critical.

When using this mechanism synthesis model to calculate the components of $\mathbf{a}_0$, $\mathbf{a}_1$, $\mathbf{b}_0$ and $\mathbf{b}_1$ (where $\mathbf{a}_0=[a_{0x},\ a_{0y},\ 1]^T$, $\mathbf{a}_1=[a_{1x},\ a_{1y},\ 1]^T$, $\mathbf{b}_0=[b_{0x},\ b_{0y},\ 1]^T$ and $\mathbf{b}_1=[b_{1x},\ b_{1y},\ 1]^T$), the user can specify a maximum of five coupler path points.

3. PLANAR FOUR-BAR MECHANISM UNDER A COUPLER LOAD

Figure 2 illustrates a statically-loaded planar four-bar mechanism. A load (vector **F**) is applied to the coupler link at **p**. To achieve static equilibrium under the coupler load **F**, the rotational degree of freedom of the crank fixed pivot (pivot $\mathbf{a}_0$) is constrained. By constraining the rotational degree of freedom of $\mathbf{a}_0$, this end of link $\overrightarrow{\mathbf{a}_0\mathbf{a}_1}$ becomes a fixed end (as indicated by the ground fixed end symbol in Figure 2). An analytical model to calculate the deflections (vector **U**) at any element node on this mechanism is formulated using

$$\{\mathbf{F}\} = \left[\mathbf{K}_{global}\right]\{\mathbf{U}\} \tag{4}$$

where the 15x15 global stiffness matrix $\left[\mathbf{K}_{global}\right]$ for the mechanism is comprised of

$$\left[\mathbf{K}_j\right] = \left[\mathbf{T}_{trans_j}\right]\left[\mathbf{k}_j\right]\left[\mathbf{T}_{trans_j}\right]^{-1} \tag{5}$$

-the element stiffness matrix for each mechanism link. In this model, the crank (link $\overrightarrow{\mathbf{a}_0\mathbf{a}_1}$) and coupler (link $\overrightarrow{\mathbf{a}_1\mathbf{p}}$ and $\overrightarrow{\mathbf{p}\mathbf{b}_1}$) are represented by beam elements. Beam elements support X and Y-deflections and Z-rotations [18]. The follower (link $\overrightarrow{\mathbf{b}_0\mathbf{b}_1}$) is represented by a truss member. Truss members support columnar deflections only [19]. The element stiffness matrix for the crank and coupler is

$$[\mathbf{k}_j] = \begin{bmatrix} \frac{A_jE_j}{L_j} & 0 & 0 & -\frac{A_jE_j}{L_j} & 0 & 0 \\ 0 & \frac{12E_jI_j}{L_j^3} & \frac{6E_jI_j}{L_j^2} & 0 & -\frac{12E_jI_j}{L_j^3} & \frac{6E_jI_j}{L_j^2} \\ 0 & \frac{6E_jI_j}{L_j^2} & \frac{4E_jI_j}{L_j} & 0 & -\frac{6E_jI_j}{L_j^2} & \frac{2E_jI_j}{L_j} \\ -\frac{A_jE_j}{L_j} & 0 & 0 & \frac{A_jE_j}{L_j} & 0 & 0 \\ 0 & -\frac{12E_jI_j}{L_j^3} & -\frac{6E_jI_j}{L_j^2} & 0 & \frac{12E_jI_j}{L_j^3} & -\frac{6E_jI_j}{L_j^2} \\ 0 & \frac{6E_jI_j}{L_j^2} & \frac{2E_jI_j}{L_j} & 0 & -\frac{6E_jI_j}{L_j^2} & \frac{4E_jI_j}{L_j} \end{bmatrix}. \quad (6)$$

Because the follower is a two-force member (and therefore under columnar loading only) its element stiffness matrix is

$$[\mathbf{k}_{axial}] = \begin{bmatrix} \frac{A_4E_4}{L_4} & 0 & 0 & -\frac{A_4E_4}{L_4} & 0 & 0 \\ 0 & 0 & 0 & 0 & 0 & 0 \\ 0 & 0 & 0 & 0 & 0 & 0 \\ -\frac{A_4E_4}{L_4} & 0 & 0 & \frac{A_4E_4}{L_4} & 0 & 0 \\ 0 & 0 & 0 & 0 & 0 & 0 \\ 0 & 0 & 0 & 0 & 0 & 0 \end{bmatrix} \quad (7)$$

The element local-to-global coordinate frame transformation matrix is

$$[\mathbf{T}_{trans_j}] = \begin{bmatrix} cos\theta_j & sin\theta_j & 0 & 0 & 0 & 0 \\ -sin\theta_j & cos\theta_j & 0 & 0 & 0 & 0 \\ 0 & 0 & 1 & 0 & 0 & 0 \\ 0 & 0 & 0 & cos\theta_j & sin\theta_j & 0 \\ 0 & 0 & 0 & -sin\theta_j & cos\theta_j & 0 \\ 0 & 0 & 0 & 0 & 0 & 1 \end{bmatrix}. \quad (8)$$

Vector **U** includes the global X and Y-deflections and Z rotations for $\mathbf{a}_0$, $\mathbf{a}_1$, $\mathbf{p}_1$, $\mathbf{b}_1$ and $\mathbf{b}_0$ (Figure 2). Because there are no global X or Y-displacements for the fixed pivots or global Z-rotations for the crank fixed pivot, these components are set to zero ($a_{0x}=a_{0y}=a_{0\theta}=b_{0x}=b_{0y}=0$). The remaining component variables are calculated from the analytical four-bar mechanism deflection model.

In Figure 2 variables E_j, A_j, I_j and L_j (where $j=1,2,3,4$) are the modulus of elasticity, cross-sectional area, moment of inertia and length of each link respectively. Because the coupler is to be a member that is uniformly rigid in this work, $E_2=E_3$, $A_2=A_3$, $I_2=I_3$ and its modulus of elasticity will be prescribed substantially higher (in this work, one million times higher) than those of the crank and follower. The angular orientation of each link (using the positive X-axis as reference) is denoted by angle θ_j (where $j=1,2,3,4$). These angles are used in Equation (8).

Equation (6) is the general stiffness matrix for beam and frame elements [18]. Each element has two nodes with three degrees of freedom per node. The first row and column in Equation (6)

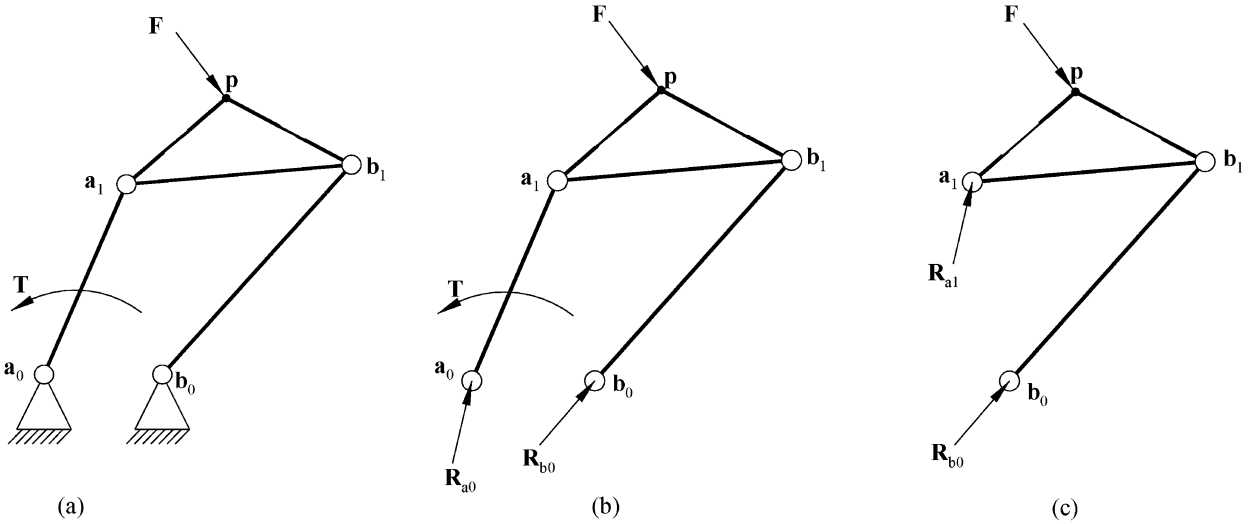

Fig. 3. (a) Four-bar mechanism in static equilibrium and (b, c) with reaction loads $\mathbf{R}_{a_0}$, $\mathbf{R}_{b_0}$ and $\mathbf{R}_{a_1}$.

correspond to the longitudinal displacements of both element nodes relative to the local element coordinate system (Figure 2). The second and third rows and columns correspond to the lateral displacements and rotations of both element nodes respectively. As nodal constraints are imposed, the general stiffness matrix includes more zero cells. For example, because the follower link of the mechanism as constrained in Figure 2 undergoes columnar loading only, its stiffness matrix (Equation (7)) only allows longitudinal displacements.

4. STATIC TORQUE CONSTRAINT OF THE CRANK LINK

With an external load **F** acting on the coupler of the planar four-bar mechanism, a driving link torque **T** achieves static equilibrium. In Figure 3a, the load **F** is applied at the arbitrary coupler point **p**. To formulate the crank link static torque constraint, the moment condition $\Sigma\mathbf{M}=0$ is considered about the fixed pivot $\mathbf{a}_0$. As illustrated in Figure 3b, the fixed pivot reaction loads $\mathbf{R}_{a_0}$ and $\mathbf{R}_{b_0}$ are also considered in the moment condition. The resulting equilibrium equation of the moments about the fixed pivot $\mathbf{a}_0$ is

$$\overrightarrow{\mathbf{a}_0\mathbf{b}_0} \times \mathbf{R}_{b_0} + \overrightarrow{\mathbf{a}_0\mathbf{p}} \times \mathbf{F} + \mathbf{T} = 0 \tag{9}$$

where

$$\mathbf{R}_{b_0} = R_b \frac{\overrightarrow{\mathbf{b}_0\mathbf{b}_1}}{\left|\overrightarrow{\mathbf{b}_0\mathbf{b}_1}\right|} \tag{10}$$

and the reaction load R_b is a real number that varies with the mechanism crank position.

By expanding the vectors $\overrightarrow{\mathbf{a}_0\mathbf{b}_0}$ and $\overrightarrow{\mathbf{a}_0\mathbf{p}}$, Equation (9) becomes

$$\left(\overrightarrow{\mathbf{a}_0\mathbf{a}_1} + \overrightarrow{\mathbf{a}_1\mathbf{b}_1} + \overrightarrow{\mathbf{b}_1\mathbf{b}_0}\right) \times \mathbf{R}_{b_0} + \left(\overrightarrow{\mathbf{a}_0\mathbf{a}_1} + \overrightarrow{\mathbf{a}_1\mathbf{p}}\right) \times \mathbf{F} + \mathbf{T} = 0. \tag{11}$$

Because link $\mathbf{b}_0\mathbf{b}_1$ is a two-force member, vectors $\mathbf{R}_{b_0}$ and $\overrightarrow{\mathbf{b}_0\mathbf{b}_1}$ are collinear and subsequently result in a zero cross product. As a result Equation (11) is simplified as

$$\left(\overrightarrow{\mathbf{a}_0\mathbf{a}_1}+\overrightarrow{\mathbf{a}_1\mathbf{b}_1}\right)\times\mathbf{R}_{b_0}+\left(\overrightarrow{\mathbf{a}_0\mathbf{a}_1}+\overrightarrow{\mathbf{a}_1\mathbf{p}}\right)\times\mathbf{F}+\mathbf{T}=0. \tag{12}$$

Next, the moment condition $\Sigma\mathbf{M}=0$ is considered about the moving pivot $\mathbf{a}_1$ considering all of the links and joints to the right of $\mathbf{a}_1$. As illustrated in Figure 3c, the fixed pivot reaction loads $\mathbf{R}_{a_1}$ and $\mathbf{R}_{b_0}$ are also considered in the moment condition. The resulting equilibrium equation of the moments about the moving pivot $\mathbf{a}_1$ is

$$\overrightarrow{\mathbf{a}_1\mathbf{b}_1}\times\mathbf{R}_{b_0}+\overrightarrow{\mathbf{a}_1\mathbf{p}}\times\mathbf{F}=0. \tag{13}$$

Substituting Equation (13) into Equation (12) produces

$$\overrightarrow{\mathbf{a}_0\mathbf{a}_1}\times\mathbf{R}_{b_0}+\overrightarrow{\mathbf{a}_0\mathbf{a}_1}\times\mathbf{F}+\mathbf{T}=0. \tag{14}$$

Substituting Equation (10) into Equation (13) and (14) produces

$$\frac{R_b}{\left|\overrightarrow{\mathbf{b}_0\mathbf{b}_1}\right|}\overrightarrow{\mathbf{a}_1\mathbf{b}_1}\times\overrightarrow{\mathbf{b}_0\mathbf{b}_1}=\mathbf{F}\times\overrightarrow{\mathbf{a}_1\mathbf{p}} \tag{15}$$

and

$$\frac{R_b}{\left|\overrightarrow{\mathbf{b}_0\mathbf{b}_1}\right|}\overrightarrow{\mathbf{a}_0\mathbf{a}_1}\times\overrightarrow{\mathbf{b}_0\mathbf{b}_1}=\mathbf{F}\times\overrightarrow{\mathbf{a}_0\mathbf{a}_1}-\mathbf{T}. \tag{16}$$

Combining Equation (15) and (16) produces

$$\mathbf{T}=\left(\frac{\left(\mathbf{F}\times\overrightarrow{\mathbf{a}_1\mathbf{p}}\right)_3}{\left(\overrightarrow{\mathbf{a}_1\mathbf{b}_1}\times\overrightarrow{\mathbf{b}_0\mathbf{b}_1}\right)_3}\overrightarrow{\mathbf{b}_0\mathbf{b}_1}+\mathbf{F}\right)\times\overrightarrow{\mathbf{a}_0\mathbf{a}_1} \tag{17}$$

where

$$\mathbf{F}=\begin{pmatrix}f_x\\f_y\\0\end{pmatrix},\quad \mathbf{T}=\begin{pmatrix}0\\0\\\tau_i\end{pmatrix},\quad \overrightarrow{\mathbf{a}_1\mathbf{p}}=\mathbf{p}_i-[\mathbf{D}_{1i}]\mathbf{a}_1,\quad \overrightarrow{\mathbf{a}_0\mathbf{a}_1}=[\mathbf{D}_{1i}]\mathbf{a}_1-\mathbf{a}_0,\quad \overrightarrow{\mathbf{b}_0\mathbf{b}_1}=[\mathbf{D}_{1i}]\mathbf{b}_1-\mathbf{b}_0,\quad \text{and}$$

$\overrightarrow{\mathbf{a}_1\mathbf{b}_1}=[\mathbf{D}_{1i}](\mathbf{b}_1-\mathbf{a}_1)$. In Equation (17) the terms $\left(\mathbf{F}\times\overrightarrow{\mathbf{a}_1\mathbf{p}}\right)_3$ and $\left(\overrightarrow{\mathbf{a}_1\mathbf{b}_1}\times\overrightarrow{\mathbf{b}_0\mathbf{b}_1}\right)_3$ are the third elements of the corresponding vectors. Equation (17) calculates the four-bar mechanism crank static torque for a given coupler load. Expressing Equation (17) as an inequality constraint to limit the maximum crank static torque for N prescribed coupler path points yields

$$(\mathbf{T}_i)^T(\mathbf{T}_i)<{\tau_{max}}^2.\ i=1,\ 2,\ 3,\ \ldots,\ N \tag{18}$$

Equation (18) is the four-bar path generator static torque constraint for the crank link.

5. FOLLOWER BUCKLING AND CRANK ELASTIC DEFLECTION CONSTRAINTS

As previously noted, the follower link is under columnar loading only because it is a two-force member. The Euler formula for critical buckling load for a column with pinned ends [18] is

$$P_{cr} = \frac{\pi^2 EI}{L^2}. \tag{19}$$

Johnson's critical buckling load formula [18] for the same system is

$$P_{cr} = \sigma_y \left(A - \frac{\sigma_y A^2 L^2}{4\pi^2 EI} \right) \tag{20}$$

where variables E, I and L are the modulus of elasticity, moment of inertia and effective column length respectively. In Equation (20) variables A and σ_y are the column cross-section area and material yield stress respectively. Solving for the columnar load in the follower link (R_b) from Equation (15) yields

$$R_b = \frac{\left| \mathbf{F} \times \overrightarrow{\mathbf{a}_1\mathbf{p}} \right|}{\left| \overrightarrow{\mathbf{a}_1\mathbf{b}_1} \times \frac{\overrightarrow{\mathbf{b}_0\mathbf{b}_1}}{|\mathbf{b}_0\mathbf{b}_1|} \right|}. \tag{21}$$

Expressing Equation (2) as an inequality constraint to prevent follower buckling for N prescribed coupler path points yields

$$([\mathbf{D}_{1i}]\mathbf{b}_1 - \mathbf{b}_0)^T ([\mathbf{D}_{1i}]\mathbf{b}_1 - \mathbf{b}_0) < \frac{\pi^2 EI}{R_b} \quad i = 1, 2, 3, \ldots, N \tag{22}$$

where the right-side quantity in this inequality is derived from Equation (19). Being a constant length constraint, Equation (22) does not calculate the follower buckling load. This equation prevents follower from reaching a buckling length when under the follower columnar load R_b.

Unlike the follower, the crank link is not a two-force member. As shown in Figure 2, the crank link is a fixed-end cantilevered beam under a transverse load that varies with crank position. The static torque applied to the crank at $\mathbf{a}_0$ (Figure 3a and 3b) and the crank reaction load at $\mathbf{a}_1$ due to $\mathbf{F}$ (Figure 3c) result in the transversely-loaded, cantilevered beam state of the crank. Because the constraint and loading conditions on the crank link make crank deflection a common occurrence, constraining the deflection of the crank is the primary concern. In this work, the buckling of link $\overrightarrow{\mathbf{a}_0\mathbf{a}_1}$ is not explicitly considered because the link stiffness required to limit transverse deflection is generally sufficient in avoiding link buckling (especially as the specified maximum transverse deflection becomes smaller).

The Euler formula for the deflection of a fixed-end cantilevered beam [18] is

$$\delta = \frac{PL^3}{3EI} \tag{23}$$

where variables P, L, E and I are the free-end transverse load, beam length, modulus of elasticity and moment of inertia respectively. From Equation (17), the total load on the moving pivot of the crank link ($\mathbf{a}_1$) is

$$\overrightarrow{\mathrm{R_a}} = \left(\frac{\left|\mathbf{F} \times \overrightarrow{\mathbf{a}_1\mathbf{p}}\right|}{\left|\overrightarrow{\mathbf{a}_1\mathbf{b}_1} \times \overrightarrow{\mathbf{b}_0\mathbf{b}_1}\right|} \overrightarrow{\mathbf{b}_0\mathbf{b}_1} + \mathbf{F} \right) \tag{24}$$

The transverse component of the crank load is

$$\overrightarrow{\mathbf{R}_{\mathbf{a}_{\mathrm{trans}}}} = \left(\frac{\left|\mathbf{F} \times \overrightarrow{\mathbf{a}_1\mathbf{p}}\right|}{\left|\overrightarrow{\mathbf{a}_1\mathbf{b}_1} \times \overrightarrow{\mathbf{b}_0\mathbf{b}_1}\right|} \overrightarrow{\mathbf{b}_0\mathbf{b}_1} + \mathbf{F} \right) \times \frac{\overrightarrow{\mathbf{a}_0\mathbf{a}_1}}{\left|\overrightarrow{\mathbf{a}_0\mathbf{a}_1}\right|} \tag{25}$$

Expressing Equation (1) as an inequality constraint to limit crank deflection for N prescribed coupler path points yields

$$([\mathbf{D}_{1i}]\mathbf{a}_1 - \mathbf{a}_0)^T([\mathbf{D}_{1i}]\mathbf{a}_1 - \mathbf{a}_0) < \left(\frac{3\delta EI}{\left|\overrightarrow{\mathbf{R}_{\mathrm{a_{trans}}}}\right|} \right)^{\frac{2}{3}} \quad i = 1, 2, 3, \ldots, N \tag{26}$$

where the right-side quantity in this inequality is derived from Equation. (22).

6. MODELING CONDITIONS AND ASSUMPTIONS

Because the mechanism of focus in this work is the planar four-bar mechanism only in-plane deflections are considered in the four-bar mechanism deflection model, crank deflection constraint and follower buckling constraint. The coupler link is assumed to be exceedingly more structurally sound than the crank and follower links, and as a result, is assumed to be a non-deforming or "rigid" member. When specifying a modulus of elasticity for the coupler link in the four-bar mechanism deflection model (Section 3), it is prescribed a value that is 1 million times higher that the modulus for the crank and follower to make its members virtually non-deforming. Also, this work only considers a force at a single coupler point. Because the system is static and the coupler point load is assumed to exceed the link body forces, these forces are neglected (massless links assumed).

7. PATH GENERATION NONLINEAR OPTIMIZATION PROBLEM

Formulating Equation (1) and (2) into a single objective function (that accommodates an indefinite number of N prescribed coupler path points) to be minimized yields

$$\begin{aligned} f(\mathbf{X}) = \sum_{i=2}^{N} \Bigg\{ & \Big[([\mathbf{D}_{1i}]\mathbf{a}_1 - \mathbf{a}_0)^T([\mathbf{D}_{1i}]\mathbf{a}_1 - \mathbf{a}_0) - (\mathbf{a}_1 - \mathbf{a}_0)^T(\mathbf{a}_1 - \mathbf{a}_0) \Big]^2 \\ & + \Big[([\mathbf{D}_{1i}]\mathbf{b}_1 - \mathbf{b}_0)^T([\mathbf{D}_{1i}]\mathbf{b}_1 - \mathbf{b}_0) - (\mathbf{b}_1 - \mathbf{b}_0)^T(\mathbf{b}_1 - \mathbf{b}_0) \Big]^2 \Bigg\} \end{aligned} \tag{27}$$

where $\mathbf{X} = \left(a_{0x}, a_{0y}, a_{1x}, a_{1y}, b_{0x}, b_{0y}, b_{1x}, b_{1y}\right)^T$. Equation (27) and inequality constraints (18), (22) and (26) constitute a nonlinear optimization problem from which mechanism solutions that approximate the prescribed coupler path points and satisfy the crank torque, crank deflection and follower buckling conditions are calculated.

The algorithm employed for solving this nonlinear optimization problem is SQP (Sequential Quadratic Programming). This algorithm uses the Quasi-Newton approach to solve its QP (Quadratic Programming) subproblem and a line search approach to determine iteration step. The merit function used by Han [20] and Powell [21] is used in the following form:

$$\Psi(\mathbf{X}) = f(\mathbf{X}) + \sum_{k=m_e+1}^{m} r_k \max[0, g_k(\mathbf{X})] \tag{28}$$

where $g_k(\mathbf{X})$ represents each inequality constraint, m_e is the total number of equality constraints ($m_e = 0$ in this work), m is the total number of inequality constraints when $m_e = 0$ and the penalty parameter is

$$r_k = (r_{l+1})_k = \max_k \left\{ \lambda_k, \frac{1}{2}\left((r_l)_k + \lambda_k\right) \right\}. \tag{29}$$

The value of r for successive minimizations can be found as

$$r_l = (\mathrm{FAC})^{\mathrm{1\text{-}IR}} \tag{30}$$

where IR=1 at the start and is incremented by 1 after each successive suboptimum is found. The factor FAC can be set arbitrarily although FAC=10 is suggested for normal use [17]. In Equation (30) l is the iteration index for calculating the penalty parameter r_k for each inequality constraint (l=0, 1, 2, 3,…). The Lagrange multiplier, which is the rate of the change of the objective function being optimized with respect to the constraint variables, is

$$\lambda_k = \frac{\nabla f(\mathbf{X})}{\nabla g_k(\mathbf{X})}. \tag{31}$$

After specifying initial guesses for the unknown variables in the optimization problem (**X**), the following SQP steps were employed to calculate the unknown variables:

1. calculate λ_k and $(r_{l+1})_k$, (where l=0 and k=1…m)
2. solve Equation (28) using Quasi-Newton method
3. calculate $(r_{l+1})_k$ using Equation (29) (where l=l+1 and k=1…m)
4. repeat step 2 with newly-calculated r_k

Steps 2 through 4 constitute a loop that is repeated until the penalty term in Equation (28), $\sum_{k=1}^{m} r_k \max[0, g_k(\mathbf{X})]$, is less than a specified penalty term residual ε (which is 0.001 for the example in this work).

Modeling the prescribed coupler path points and concept mechanisms via CAD software could enable one to specify initial guesses for the unknown mechanism more judiciously than by arbitrary guessing. This approach could improve the SQP programming results since SQP Programming does not guarantee global optimization.

8. PATH GENERATOR SELECTION ALGORITHM

Martin et al. [1] presented a selection algorithm for planar four-bar motion generators that considers Grashof conditions, transmission angles and mechanism perimeters. The algorithm

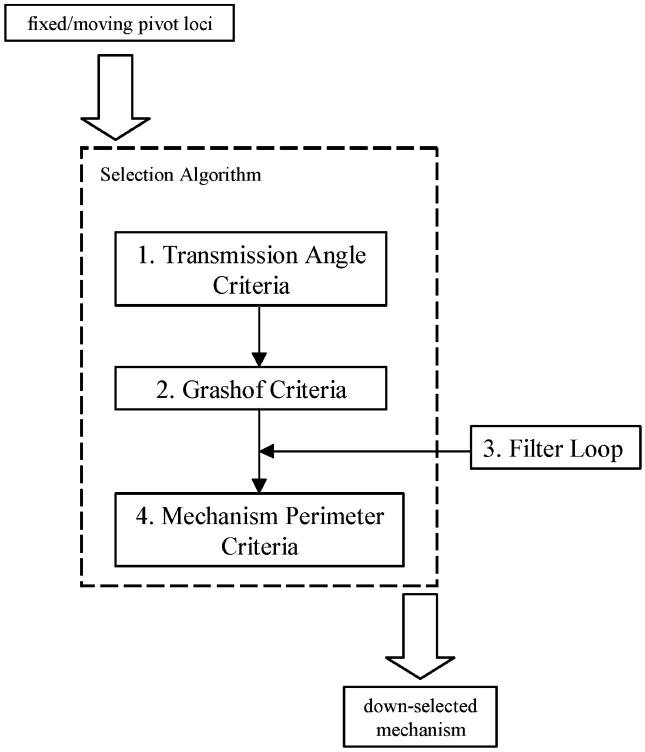

Fig. 4. Planar four-bar path generator selection algorithm diagram.

input are the fixed and moving pivot solutions calculated for a set of prescribed coupler path points. The algorithm down-selects mechanism solutions according to the specified Grashof mechanism type, transmission angle range and mechanism perimeter condition.

In its original form, the algorithm presented by Martin et al. [1] requires a single fixed pivot locus and a single moving pivot locus as input. The optimization problem on the other hand calculates four loci (one locus each for $\mathbf{a}_0$ $\mathbf{a}_1$, $\mathbf{b}_0$ and $\mathbf{b}_1$). When a continuous fixed pivot locus and moving pivot locus are read into the macro codified under the original algorithm, a combination of valid and invalid mechanism solutions are produced. A filter loop (block 3 in Figure 4) will exclude the invalid solutions prior to the mechanism perimeter loop (block 4 in Figure 4). The filter loop codified in MathCAD is included in the Appendix. The user should insert the filter loop immediately after the Grashof criteria loop as shown in Figure 4 to update the original selection algorithm code.

9. PATH GENERATION EXAMPLE

Table 1 includes the X and Y-coordinates (in meters) of 8 prescribed coupler path points and arbitrary coupler displacement angles. The maximum allowed crank torque is τ_{max} = 248N-m and the coupler load at $\mathbf{p}$ is $\mathbf{F}=(0, -4448, 0)^T$N. In this example, the coupler load represents an external force. The crank and follower links shall be constructed of solid circular steel (E=200GPa) tubing of $1.9050*10^{-2}$m and $0.4762*10^{-2}$m diameters respectively. For each prescribed coupler points, the maximum crank deflection shall not exceed $3.30*10^{-4}$m and avoiding follower buckling is critical.

Table 1. Prescribed and achieved coupler path points.

	$\mathbf{p}_{prescribed}$ [m]	$\alpha_{prescribed}$ [deg]	$\mathbf{p}_{achieved}$ [m]	$\alpha_{achieved}$ [deg]
Pos 1	0.129357, 0.129967	0	0.129418, 0.129936	0
Pos 2	0.113873, 0.134630	−1.5125	0.113995, 0.135758	4.5991
Pos 3	0.096378, 0.135545	−2.431	0.095829, 0.136428	8.0984
Pos 4	0.078395, 0.132283	−2.9232	0.078303, 0.131582	10.6369
Pos 5	0.027371, 0.091013	−0.8910	0.043373, 0.088026	12.2871
Pos 6	0.015819, 0.064618	5.7509	0.043861, 0.071780	6.9920
Pos 7	0.037338, 0.047701	47.6085	0.049500, 0.061417	5.3094
Pos 8	0.073061, 0.073731	46.8257	0.074341, 0.056815	−12.1069

Figure 5 illustrates the fixed and moving pivot loci calculated using the nonlinear optimization problem with a prescribed range of b_{0x} = −0.0508, −0.0495…0.0508m and initial guesses (in meters) of b_{0y} =0, $\mathbf{b}_1$=(0.0381, 0.0635), $\mathbf{a}_0$=(0.1651, 0.0127) and $\mathbf{a}_1$=(0.1905, 0.1016). The fixed and moving pivot loci are used as input for the updated selection algorithm with a transmission angle range of 40°≤trans.≤140°, the Grashof crank-rocker condition and a minimum mechanism perimeter condition. The resulting dimensions (in meters) for the path generator selected (Figure 5 and 7) are $\mathbf{b}_0$=(0.038100, −0.021057), $\mathbf{b}_1$=(0.016739, 0.074854), $\mathbf{a}_0$=(0.147879, 0.090703) and, $\mathbf{a}_1$=(0.183490, 0.128194). This mechanism has crank, coupler, follower and ground lengths of 0.051707, 0.175074, 0.098260 and 0.156657 meters respectively (satisfying Grashof crank-rocker conditions) and produces the transmission profile illustrated in Figure 6. Figure 7 also includes the coupler path points achieved by the synthesized path generator. This mechanism is the most compact of the available solutions (satisfying minimum

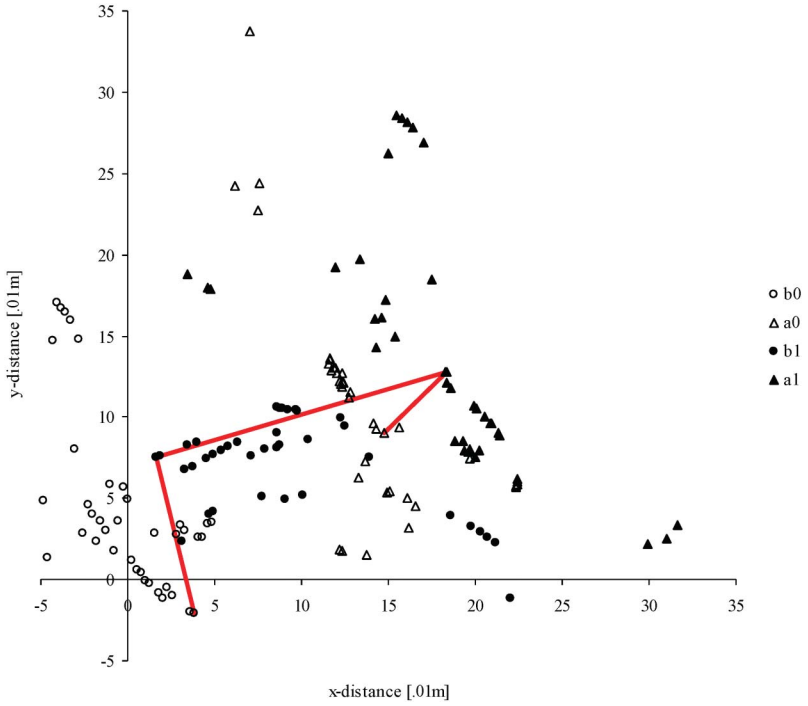

Fig. 5. Path generator fixed and moving pivot loci (with mechanism selection superimposed).

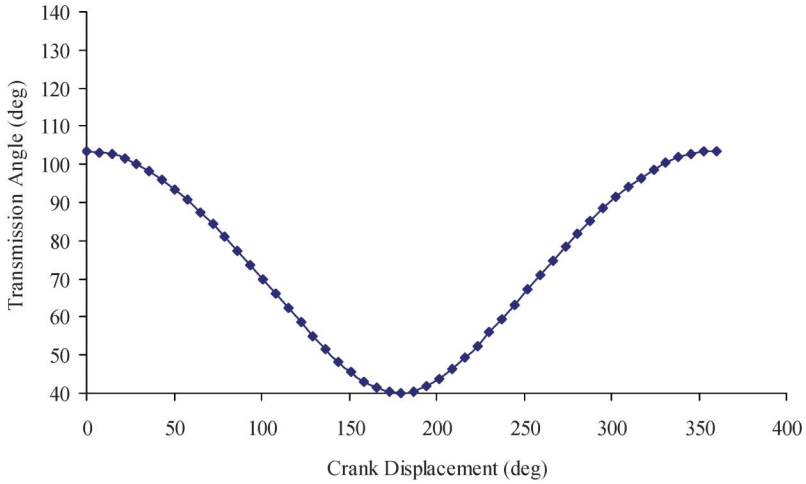

Fig. 6. Path generator transmission angles.

perimeter condition). Table 2 includes the resulting static torque and deflection of the crank link as well as the resulting follower link columnar loads. The follower buckling load is 6512N. As noted in Section 5, the link stiffness required to limit transverse deflection for link $\overrightarrow{\mathbf{a}_0\mathbf{a}_1}$ is generally sufficient in avoiding buckling. The calculated buckling load for link $\overrightarrow{\mathbf{a}_0\mathbf{a}_1}$ is over 4MN-far exceeding the applied coupler load.

Because the crank and follower links are elastic, the deflections of these links compromise the accuracy of the coupler path points achieved by the synthesized mechanism. Table 1 includes the coupler path points and orientation angles calculated from the mechanism deflection model in Section 3. Because coupler point accuracy is the focus in path generation, the accuracy of the orientation angles approximated by the synthesized mechanism is not critical. Figure 8 is a plot of the scalar differences between the prescribed and achieved coupler path points ($|\mathbf{p}_{prescribed}\text{-}\mathbf{p}_{achieved}|$). Coupler path points 1 through 8 correspond to crank angles of $\theta_1=$

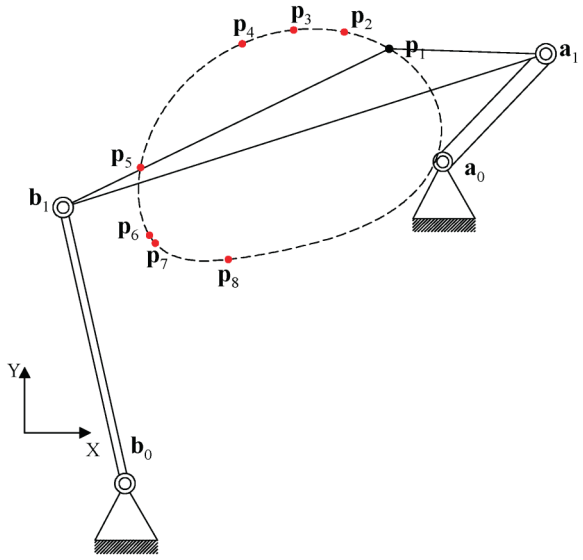

Fig. 7. Coupler path points achieved by synthesized path generator.

Table 2. Crank static torques, deflections and follower columnar loads.

	Crank Static Torque [N-m]	Crank Deflection [10^{-4}m]	Follower Load [N]
Pos 1	99.20	0.69	1378.94
Pos 2	42.26	0.28	1378.94
Pos 3	27.23	0.18	1370.05
Pos 4	95.25	0.66	1378.94
Pos 5	210.49	1.45	1801.52
Pos 6	177.27	0.99	2375.34
Pos 7	110.50	0.84	2473.20
Pos 8	26.89	0.18	2348.66

133.5271°, 112.8409°, 92.5959°, 72.2693°, 8.6884°, 336.4193°, 331.0413° and 294.6046° respectively.

As a comparison between the structural integrity of a path generator calculated using the nonlinear optimization problem and a path generator calculated using Equation (1) and (2) alone, a solution was calculated using the latter model. A prescribed value of $a_{0x} = 0$, the first four coupler precision points in Table 1 and initial guesses of $a_{0y} = 0$, $\mathbf{a}_1 = (0.0381, 0.0635)$, $\mathbf{b}_0 = (0.1651, 0.0127)$ and $\mathbf{b}_1 = (0.1905, 0.1016)$ resulted in $a_{0y} = 0.020574$, $\mathbf{a}_1 = (0.035052, 0.079756)$, $\mathbf{b}_0 = (0.367792, 0.011938)$ and $\mathbf{b}_1 = (0.365252, 0.164846)$. Because the conventional model includes no constraints for buckling and deflection, the calculated four-bar mechanism solution has a follower scalar length of 0.152908m which is substantially longer than the follower from the optimization problem solution and much more susceptible to buckling (2131N vs. 6512N in the optimization problem). In addition, the conventional model does not ensure full link rotatibility or feasible transmission angles. Although it is possible to calculate a kinematically and structurally sound mechanism solution from the convention method by trial and error, the nonlinear optimization problem produces solutions that are kinematically and structurally sound specifically.

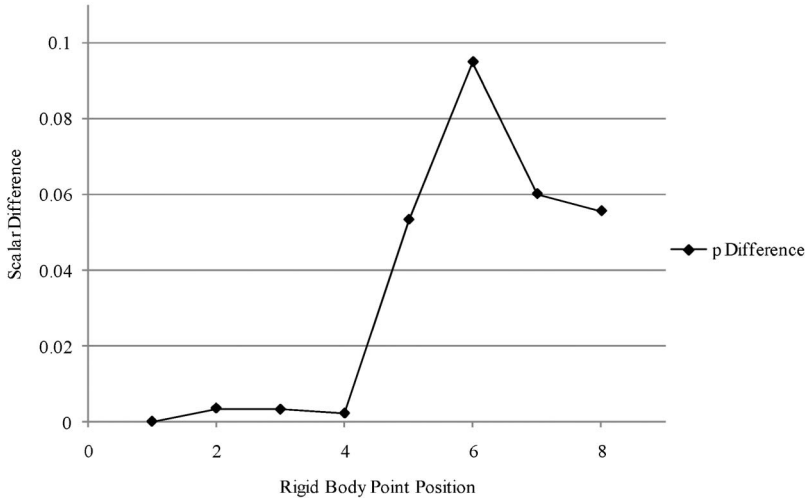

Fig. 8. Scalar differences between prescribed and achieved coupler path points.

10. DISCUSSION

In the example problem, the authors prescribed 8 coupler path points. Because the nonlinear optimization problem formulated in this work can theoretically accommodate an indefinite number of precision points, the user is not limited to 8 points. Equation (17) becomes invalid when the pivots $\mathbf{a}_1$, $\mathbf{b}_1$ and $\mathbf{b}_0$ are collinear because when collinear, the denominator in Equation (17) becomes zero. Such a state is possible when the four-bar mechanism reaches a ''lock-up'' or binding position. The mathematical analysis software *MathCAD* was used to codify and solve the formulated nonlinear optimization problem. The cross-sectional area of the follower link, its slenderness ratio and the column constant determine whether Euler's or Johnson's buckling formula (Equation (19) and (20) respectively) is used. By substituting Euler's buckling formula with Johnson's critical buckling load formula, Equation (22) could be reformulated to consider the latter buckling condition.

11. CONCLUSION

Although the assumption of link rigidity in kinematic synthesis may be generally appropriate and often practiced, a mechanism under a coupler load will undergo a degree of elastic deflection-particularly the crank and follower links. Excessive crank deflection and follower buckling can compromise the accuracy of the precision points approximated and should be considered in path generation where coupler loads exist. This work demonstrates the synthesis of a planar four-bar path generator with respect to the following conditions:

- Grashof conditions, transmission angle ranges and mechanism perimeter conditions
- Crank static torque condition
- Crank elastic deflection and follower buckling conditions.

Both the nonlinear optimization problem and modified algorithm ran efficiently in *Mathcad*-having run times measuring in seconds.

REFERENCES

1. Martin, P.J., Russell, K. and Sodhi, R.S., ''An algorithm for planar four-bar motion generation with optimization,'' *Transactions of the Canadian Society for Mechanical Engineers*, Vol. 31, No. 3, pp. 357–371, 2007.
2. Yao, J. and Angeles, J., ''Computation of all optimum dyads in the approximate synthesis of planar linkages for rigid-body guidance,'' *Mechanism and Machine Theory*, Vol. 35, No. 8, pp. 1065–1078, 2000.
3. Hong, B. and Erdman, A.G., ''A method for adjustable planar and spherical four-bar linkage synthesis,'' *ASME Journal of Mechanical Design*, Vol. 127, No. 3, pp. 456–463, 2005.
4. Zhou, H. and Cheung, E.H.M., ''Adjustable four-bar linkages for multi-phase motion generation,'' *Mechanism and Machine Theory*, Vol. 39, No. 3, pp. 261–279, 2004.
5. Al-Widyan, K., Angeles, J. and Jesús Cervantes-Sánchez, J., ''The robust synthesis of planar four-bar linkages for motion generation,'' *Proceedings of the ASME Design Engineering Technical Conference 5 A*, pp. 627–633, 2002.
6. Danieli, G.A., Mundo, D. and Sciarra, V., ''Use of Burmester's circular theory in the determination of the optimal four-bar link reproducing actual tibia-femur relative motion,'' *ASME Bioengineering Division, BED 51*, pp. 97–98, 2001.

7. Goehler, C.M., Stanisic, M.M. and Perez, V.P., "A generalized parameterization of T_1 motion and its applications to the synthesis of planar mechanisms," *Mechanism and Machine Theory*, Vol. 39, No. 11, pp. 1223–1241, 2004.
8. Caracciolo, R. and Trevisani, A., "Simultaneous rigid-body motion and vibration control of a flexible four-bar linkage," *Mechanism and Machine Theory*, Vol. 36, No. 2, pp. 221–243, 2001.
9. Zhixing, W., Hongying, Y., Dewei, T. and Jiansheng, L., "Study on rigid-body guidance synthesis of planar linkage," *Mechanism and Machine Theory*, Vol. 37, No. 7, pp. 673–684, 2002.
10. Lin, S. and Modler, K.H., "Path generation with emphasis on desired mechanism type and characteristics," *Proc. of the 11th World Congress in Mechanism and Machine Science*, China Machine Press, Tianjin, China, Vol. 3, pp. 1264–169, 2004.
11. Huang, C. and Roth, B., "Dimensional synthesis of closed-Loop linkages to match force and position specifications," *Journal of Mechanical Design*, Vol. 115, pp. 194–198, 1993.
12. Dado, M.H.F., "Limit position synthesis and analysis of compliant 4-bar mechanism with specified energy levels using parametric pseudo-rigid-body model," *Mechanism and Machine Theory*, Vol. 40, No. 1, pp. 977–992, 2005.
13. Venanzi, S., Giesen, P. and Parenti-Castelli, V., "A novel technique for position analysis of planar complaint mechanisms," *Mechanism and Machine Theory*, Vol. 40, No. 11, pp. 1224–1239, 2005.
14. Sönmez, Ü., "Introduction to compliant long dwell mechanism designs using buckling beams and arcs," *Journal of Mechanical Design*, Vol. 129, No. 8, pp. 831–843, 2007.
15. Plaut, R.H., Alloway, L.A. and Virgin, L.N., "A nonlinear oscillations of a buckled mechanism used as a vibration isolator," *Proceedings of the IUTAM Symposium*, Vol. 122, pp. 241–250, 2003.
16. Sriram, B.R. and Mruthyunjaya, T.S., "Synthesis of path generating flexible-link mechanisms," *Computer and Structures*, Vol. 56, No. 4, pp. 657–666, 1995.
17. Suh, C.H. and Radcliffe, C.W., *Kinematics and Mechanism Design*, John Wiley and Sons Inc., New York, 1978.
18. Pilkey, W.D., *Formulas for Stress, Strain and Structural Matrices*, John Wiley and Sons Inc., New York, 1994.
19. Moaveni, S., *Finite Element Analysis Theory and Application with ANSYS*, Prentice-Hall, Englewood Cliffs, 1999.
20. Han, S.P., "A Globally Convergent Method for Nonlinear Programming," *J. Optimization Theory and Applications*, Vol. 22, p. 297, 1977.
21. Powell, M.J.D., "A Fast Algorithm for Nonlinearly Constrained Optimization Calculations," Numerical Analysis, G. A. Watson ed., Lecture Notes in Mathematics, Springer-Verlag, Berlin, Vol. 630, 1978.

APPENDIX

Filter loop (codified in *MathCAD*) for planar four-bar motion generator selection algorithm

```
Cell:= | M←stack(∞ ∞ ∞ ∞)
       | for i ∈ 1…rows(Cell) −1
       |   | M1←(Cell_{i,0} Cell_{i,1} Cell_{i,2} Cell_{i,3})
       |   | for j ∈ 0…(end/2) −1
       |   |   | continue if (Cell_{i,0} ≠ CRANK_j)
       |   |   | M1←(∞ ∞ ∞ ∞) if Cell_{i,2} ≠ CRANK_{j+(end/2)}
       |   |   | M←stack(M, M1)
       | M
```